Available online at www.sciencedirect.com
SCIENCE DIRECT®
Journal of Catalysis 222 (2004) 107–116
JOURNAL OF CATALYSIS
www.elsevier.com/locate/jcat

Tertiary butylation of phenol on $Cu_{1-x}Co_xFe_2O_4$: catalysis and structure–activity correlation

Thomas Mathew, Bollapragada S. Rao, and Chinnakonda S. Gopinath *

Catalysis Division, National Chemical Laboratory, Dr. Homi Bhabha Road, Pune 411 008, India

Received 7 July 2003; revised 24 November 2003; accepted 1 December 2003

Abstract

A systematic study of catalytic tertiary butylation of phenol was carried out with isobutene as a function of temperature, feed composition, time on stream, space velocity, and catalyst composition on $Cu_{1-x}Co_xFe_2O_4$ ($x = 0$ to 1) system. Tertiary butylation of phenol gives three products, namely, 2-*tert*-butyl phenol, 4-*tert*-butyl phenol, and 2,4-di-*tert*-butyl phenol. The phenol conversion and selectivity of these products depend on the reaction parameters. A good correlation was found between the activity, in terms of phenol conversion and various product selectivities for this reaction, and the acid–base properties of the catalysts. High activity is achieved with $x = 0.5$ composition, illustrating the importance of a 1:1 combination of Cu and Co and the necessity for optimum concentrations of acid–base centers for this reaction. A reaction mechanism involving the interaction of phenoxide from phenol and the *tert*-butyl cation from isobutene on $Cu_{1-x}Co_xFe_2O_4$ is proposed. X-ray photoelectron spectroscopy and X-ray induced Auger electron spectroscopic analysis of fresh and spent catalysts revealed a partial reduction of metal ions due to reaction. Valence band studies clearly revealed an increase in the overlap of metal ion 3*d* bands from fresh to spent catalysts as reflected from a large decrease in the energy gap between them. The better catalytic results observed with $x = 0.5$ are attributed to an optimum distribution of Cu species with heteroatom neighbors, maximum overlap between the Cu and Co 3*d* bands, and intermediate acid–base character.

Keywords: Tertiary butylation; Phenol; $Cu_{1-x}Co_xFe_2O_4$; Ferrospinel; X-ray photoelectron spectroscopy; Acidity; Basicity; Acid–base pair; Valence band overlap; Metal ion distribution

1. Introduction

Tertiary butylation of phenol has been studied extensively owing to industrial interest in the production of a variety of materials [1]. For example, 2-tertiary butylphenol (2-tBP) is a starting material for the synthesis of antioxidants and agrochemicals. Triphosphate and benzotriazole derivatives of 2,4-ditertiary butylphenol (2,4-dtBP) are employed as costabilizers for polyvinyl chloride and UV absorbers in polyolefins, respectively. Various catalysts reported for tertiary butylation of phenol include Cr_2O_3, ion-exchange resins, ZrO_2, sulfated zirconia, aluminum hydrotalcites, molecular sieves, and zeolites including mordenite, SAPO-11, HY, Hβ, AlMCM-41, and FeMCM-41 [2–14]. Unlike other phenol alkylation, tertiary butylation of phenol gives numerous products including 3-*tert*-butylphenol depending on the catalysts and on the reaction conditions. Most of the above-mentioned catalysts are focused on the production of 4-tertiary butylphenol (4-tBP), 2,4-dtBP, and 2,6-dtBP. 2-tBP is produced as the main product of phenol butylation with isobutene in the presence of an acidic ion-exchange resin catalyst [1]. Though cation exchange resin catalysts have an advantage due to environmental friendliness, they have disadvantages due to tedious workup, less activity, and less stability at high temperatures.

Ferrites of spinel-type structure are found to be highly active toward many aromatic alkylation reactions such as phenol alkylation, aniline methylation, and pyridine methylation [15–19]. The catalytic effectiveness of these systems is due to the ability of the metallic ions to migrate between the sublattices without altering the structure, which makes the catalyst efficient for many organic transformation reactions. The $Cu_{1-x}Co_xFe_2O_4$ system was found to be highly active for phenol alkylation with different alkylating agents and has been characterized in detail [19–23]. The prime attraction of this catalyst system is its high *ortho* products

* Corresponding author.
E-mail address: gopi@cata.ncl.res.in (C.S. Gopinath).

0021-9517/$ – see front matter
doi:10.1016/j.jcat.2003.12.001

selectivity with high phenol conversion. Cu–Co combination in terms of synergism and 3*d* energy band overlap were suggested to be responsible for this efficient process [21]. As part of continuing studies on alkylation in our laboratory, we carried out tertiary butylation of phenol with isobutene (IB). Effects of various parameters such as reaction temperature, time on stream (TOS), space velocity, mole ratio of phenol to IB, and catalyst composition were studied. Effects of these parameters on phenol conversion and selectivity to various products were also studied. A good correlation was found between activity, in terms of phenol conversion and selectivity of various products for this reaction, and the acid–base properties of the catalysts. Special attention was paid to the associated changes in terms of surface composition and the overall electronic structure of catalysts due to reaction.

2. Experimental

$Cu_{1-x}Co_xFe_2O_4$ ($x = 0$, 0.25, 0.50, 0.75, and 1) samples were prepared by coprecipitation technique and characterized by various physicochemical techniques as reported in earlier articles [20–23]. Briefly, stoichiometric amounts of premixed metal nitrate solutions were added to NaOH solution with continuous stirring. The final pH of the resulting solution was adjusted to between 9.5 and 10. The precipitate was washed with demineralized water until Na^+ and NO_3^- ions disappeared. The precipitates were filtered, dried at 80 °C, and calcined at 500 °C. The chemical compositions of calcined (fresh) catalysts were determined by X-ray fluorescence (XRF) spectroscopy. X-ray diffraction (XRD) patterns of the powder catalysts were recorded with Cu-K_α radiation ($\lambda = 1.5405$ Å) with a Ni filter to obtain unit cell parameter (a) and crystallite size. The BET surface area and pore volume of the catalysts were determined by a N_2 adsorption–desorption method at 77 K using a Quantachrome NOVA-1200 adsorption unit. For X-ray photoelectron spectroscopy (XPS) measurements, a VG Microtech Multilab ESCA 3000 spectrometer with a non-monochromatized Mg-K_α X-ray source ($h\nu = 1253.6$ eV) was employed with in situ scraped fresh catalyst pellets and powder samples of spent catalysts. Energy resolution of the spectrometer was set at 0.8 eV with Mg-K_α radiation at a pass energy of 20 eV. Binding energy calibration was performed with the Au $4f_{7/2}$ core level at 83.9 eV. Spent catalysts analyzed by XRD and XPS, after butylation at 200 °C for 10 h, had a 1:3 composition of PhOH:IB, unless otherwise stated.

The reactions were conducted in a vapor-phase setup at atmospheric pressure in a vertical, downflow, fixed-bed glass reactor 17–18 mm in internal diameter. This glass reactor was placed inside a split-type furnace (Geomechanique, France), which can maintain different temperatures in the upper and lower halves [22]. Three grams of fresh catalyst with a particle size around 20 mesh (different particle sizes did not have any significant effect on the kinetic results reported here) was charged each time in the center of the reactor in such a way that the catalyst was sandwiched between the layers of inert porcelain beads. The upper portion of the reactor was also filled with inert beads and served as a vaporizer-cum-preheater; it was maintained at 200 °C or the reaction temperature, whichever was higher, to ensure that phenol was fully vaporized before it reached the catalyst bed. The feed mixture containing phenol and IB gas in the appropriate ratio was passed simultaneously. IB flow was measured with a mass flow controller. Phenol was heated at 55 °C and pumped through a syringe pump (ISCO, Model 500D). The feed line from the pump to the reactor was also heated at 55 °C. The products were collected in a condenser cooled with ice-cold water and the analysis was performed with GC, GC-MS, and GC-IR methods. The accuracy of the catalytic activity values reported in this article was determined by repeated measurements and is reproducible within ±5%.

3. Results

3.1. Characterization of $Cu_{1-x}Co_xFe_2O_4$

Catalysts were characterized with respect to chemical composition structural and textural properties have already been reported [20–23]. In Fig. 1 shows the XRD patterns of calcined (a) and spent (b) catalysts. Fresh Cu-rich catalyst ($x = 0$) exhibits a diffraction pattern attributed to cubic spinel phase and a considerable amount of CuO and Fe_2O_3. Substitution of Cu with Co increases the overall crystallinity of the spinel phase and all the peaks are indexed (ASTM Card Nos. 1-1121 and 3-0864). The XRD pattern of spent catalysts displays Cu^0 at $x = 0$ along with CuO and Fe_2O_3; however, only a trace amount of Cu^0 is detected at $0.25 \leqslant x \leqslant 0.75$ and there is no major change on $CoFe_2O_4$ after reaction. Table 1 lists the unit cell values (a) for all catalysts, which decrease with increasing x. Deviation at $x = 0$ composition is due mainly to the significant amount of impurities present. Surface area and pore volume (Table 1) have relatively high values at $x = 0.5$; however, other compositions, except $x = 0.0$, are associated with comparable values, hinting that there might be no major influence of textural properties on catalytic properties. Relative acidity and basicity values were measured from the pyridine and CO_2 adsorbed on the catalyst surfaces at 100 °C and room temperature, respectively [23]. A systematic increase (decrease) in relative acidity (basicity) is observed with increasing x value.

3.2. Catalytic activity studies

3.2.1. Effect of isobutene:phenol mole ratio

Tertiary butylation of phenol was carried out at 200 °C with various IB:phenol mole ratios (IB:PhOH) between 1 and 7 on $Cu_{0.5}Co_{0.5}Fe_2O_4$ to determine the optimum feed ratio (Fig. 2a). The main products of tertiary butylation of

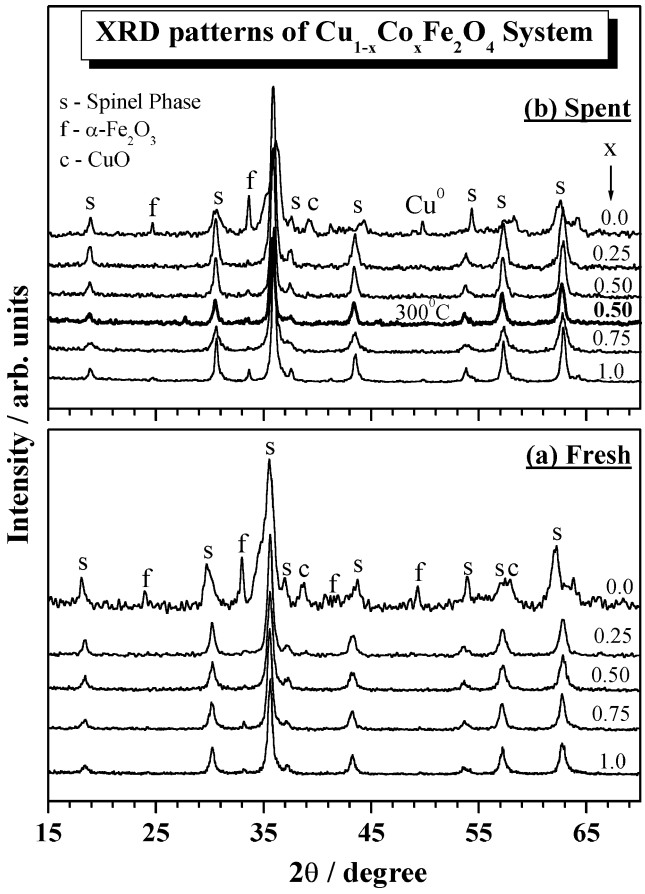

Fig. 1. X-ray diffractograms of (a) fresh and (b) spent $Cu_{1-x}Co_xFe_2O_4$ catalysts. X-ray diffractogram of spent catalysts were obtained after tertiary butylation of phenol at 200 °C for 10 h with a 1:3 composition of phenol:isobutene. Note that a significant amount of metallic Cu is seen for $x = 0.0$ spent catalyst.

Table 1
Textural and acid–base characteristics of $Cu_{1-x}Co_xFe_2O_4$

Composition, x	a (Å)	S_{BET} (m^2/g)	Pore volume (cc/g) (10^{-2})	Relative acidity (basicity)[a]
0.0	8.3898	28.8	5.1	300 (580)
0.25	8.4051	34.0	6.7	381 (510)
0.50	8.4012	43.8	10.9	479 (420)
0.75	8.3982	36.6	6.4	623 (275)
1.0	8.3997	36.8	5.9	782 (210)

[a] Obtained from FT-IR studies of pyridine and CO_2 adsorbed catalysts [23].

phenol are 2-tBP, 4-tBP, and 2,4-dtBP. A trace amount of 2,6-dtBP is also formed. It can be seen that phenol conversion increases as the IB:PhOH increases to 3 and thereafter marginally increases to 5 and then decreases. However, comparatively high yields of 2-tBP and 2,4-dtBP were observed at a feed ratio of 3:1. Further, too much of either of the reactants in the feed deactivates the catalyst rapidly, hence an optimum feed ratio of 3:1 was maintained for further studies. It is to be noted that the amount of unreacted IB increases with increasing feed ratio. Concurrently, there is an increase

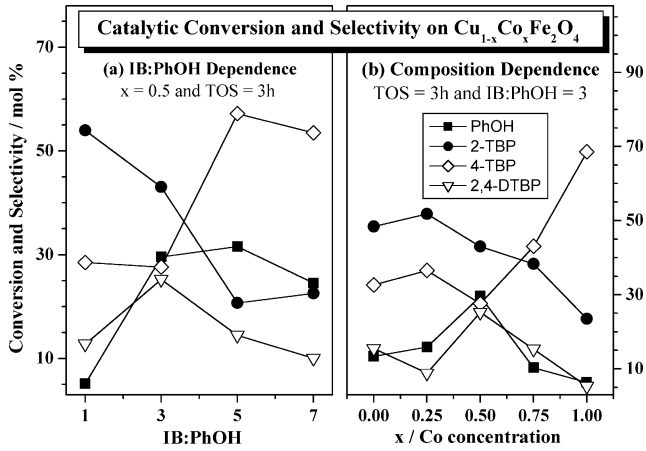

Fig. 2. (a) Isobutene:phenol feed composition dependence of phenol conversion and selectivity of all tertiary butylation products on $Cu_{0.5}Co_{0.5}Fe_2O_4$, at 200 °C and TOS of 3 h. (b) Catalyst composition dependence of phenol conversion and selectivity of tertiary butylation products at 200 °C and IB:PhOH of 3 are shown for $Cu_{1-x}Co_xFe_2O_4$. Note an increase in the selectivity of 4-*tert*-butylated phenol with increase in Co content and increase in isobutene in the feed.

Table 2
Influence of catalyst composition on phenol conversion and product distribution over $Cu_{1-x}Co_xFe_2O_4$ ($x = 0$, 0.25, 0.50, 0.75 and 1)[a]

Product distribution (mol%)	Catalyst composition, x				
	0	0.25	0.50	0.75	1
2-*tert*-butyl phenol	6.49	8.25	12.76	3.97	1.50
4-*tert*-butyl phenol	4.38	5.83	8.19	4.46	4.37
2,4-Di-*tert*-butyl phenol	2.08	1.41	7.49	1.59	0.34
2,6-Di-*tert*-butyl phenol	0.17	0.13	0.48	0.12	0
Others (including *o*-cresol and 2,6-xylenol)	0.29	0.30	0.70	0.20	0.16
Phenol conversion	13.40	15.92	29.62	10.34	6.37
2-*tert*-butyl phenol selectivity	48.43	51.82	43.08	38.39	23.55
4-*tert*-butyl phenol selectivity	32.69	36.62	27.65	43.13	68.60
2,4-Di-*tert*-butyl phenol selectivity	15.52	8.86	25.29	15.38	5.34
Total *ortho* selectivity	49.70	52.64	44.70	39.45	23.55

[a] Phenol butylation is carried out at a phenol:isobutene mole ratio of 1:3 at 200 °C and a WHSV of 1 h^{-1}.

in the amount of aliphatics formed (results not shown) due to oligomerization as well as cracking of IB. 4-tBP selectivity increases as IB:PhOH increases up to 5 and thereafter marginally decreases. Though the selectivity of 4-tBP increased with a large amount of IB in the feed, there is a perceptible drop in the selectivity of both 2-tBP and 2,4-dtBP.

3.2.2. *Effect of catalyst composition*

Fig. 2b illustrates the catalyst composition dependence of phenol conversion and selectivity of tertiary butylated phenols on $Cu_{1-x}Co_xFe_2O_4$ at 200 °C with IB:PhOH mole ratio of 3:1 and WHSV of 1 h^{-1}. Conversion and product selectivity of phenol tertiary butylation on $Cu_{1-x}Co_xFe_2O_4$ under optimum conditions are also summarized in Table 2. The important observations are: (1) Phenol conversion increases from $x = 0$ to 0.5 and then decreases with further increase in x. (2) 2-tBP selectivity decreases as Cu con-

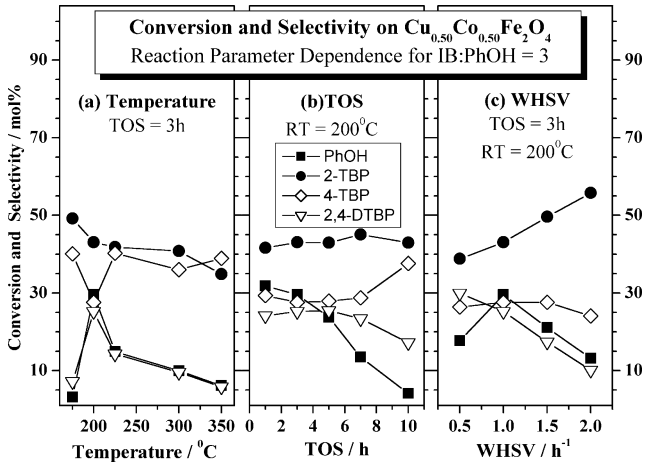

Fig. 3. Tertiary butylation of phenol is shown on $Cu_{0.5}Co_{0.5}Fe_2O_4$, with IB:PhOH = 3, as a function of (a) reaction temperature, (b) time on stream, and (c) weight hourly space velocity.

tent decreases. (3) 4-tBP selectivity increases at $x > 0.5$, however, with a concurrent decrease in phenol conversion. (4) $x = 0.5$ is associated with maximum phenol conversion and high selectivity towards 2,4-dtBP formation. A sudden increase in 2,4-dtBP and a parallel decrease in 2-tBP selectivity at $x = 0.5$ hints that tertiary butylation is sequential.

3.2.3. Effect of reaction temperature

Fig. 3a shows the effect of reaction temperature on the conversion of phenol and selectivity of various products on $x = 0.5$ at a space velocity of 1 h^{-1} and TOS of 3 h. Phenol conversion increases from 175 to 200 °C and afterward falls at high temperatures. Maximum phenol conversion is observed at 200 °C. Phenol conversion increases from 3 to 30 mol% as the temperature changes from 175 to 200 °C. The one-to-one change observed between phenol conversion and 2,4-dtBP selectivity indicates the first-order dependence of phenol conversion on 2,4-dtBP yield. An increase in temperature does not change 2-tBP selectivity significantly. 4-tBP selectivity also remains the same from 175 to 350 °C, except at 200 °C. A significant increase in 2,4-dtBP selectivity at the cost of 4-tBP and 2-tBP selectivity indicates again that at high phenol conversion, the reaction pattern shifts significantly to ditertiary butylation; this point is worth investigating further. It is found that as the temperature increases, the amount of unreacted IB decreases and the amounts of aliphatics increase.

3.2.4. Effect of time on stream

The effect of TOS is expected to shed light on deactivation of any catalyst and its influence on product selectivity. Since $x = 0.50$ was found to be a better catalyst for the phenol tertiary butylation reaction, the TOS dependence of this catalyst at 200 °C was investigated and is shown in Fig. 3b. It was found that the conversion of phenol is high up to 5 h and then decreases significantly. The selectivity of 2-tBP remains constant at 45 mol% irrespective of TOS. The selectivity of 4-tBP and 2,4-dtBP also remains the same, around 25–30 mol%, up to 8 h; however, the selectivity changes after 8 h. It is to be noted here also that phenol conversion and 2,4-dtBP selectivity vary hand-in-hand, as in the temperature dependence studies.

3.2.5. Effect of weight hourly space velocity (WHSV)

The effect of WHSV on catalytic performance was studied in the range 0.5–2 h^{-1} using the $x = 0.5$ catalyst at 200 °C (Fig. 3c). It can be seen from the data that both high WHSV and low WHSV are not helpful for high catalytic performance. Phenol conversion is maximum at an optimum WHSV of 1 h^{-1}. High phenol conversion with a good yield of 2-tBP is achieved at a WHSV of 1–1.5 h^{-1}. It was also found that 2,4-dtBP selectivity decreases with increasing WHSV. Addition of 2-tBP and 2,4-dtBP selectivity gives a constant value of 67 mol% independent of WHSV values, strongly indicating that tertiary butylation is sequential and tertiary butylation at the *ortho* position takes place first followed by a second tertiary butylation at the *para* position. This also suggests that there is no isomerization between 2-tBP and 4-tBP. 4-tBP selectivity does not show significant WHSV dependence.

3.3. XPS analysis

XPS has been used to examine the changes in oxidation state and surface composition of catalysts. Spent catalyst of $x = 0.5$ composition obtained after reaction for 10 h with a 1:3 ratio of IB:PhOH at 300 °C (hereafter, $x = 0.5$@300 °C) was also subjected to XPS analysis.

3.3.1. Cu 2p core level and Cu–$L_3M_{45}M_{45}$

Photoemission spectra from the Cu $2p_{3/2}$ core level for both fresh and spent $Cu_{1-x}Co_xFe_2O_4$ catalysts are shown in Figs. 4a and b, respectively. It is clear that all fresh catalysts exhibit the Cu $2p_{3/2}$ main peak at a binding energy (BE) of 934.2 ± 0.2 eV with good satellite intensity (I_S) around 942 eV, confirming the existence of Cu^{2+}. The intensity of satellite to mainline (I_S/I_M) is between 0.5 and 0.6 in all cases (Fig. 4d), which is very close to that of CuO (0.55) [24]. The above facts indicate the charge density on Cu is the same at all catalyst compositions.

Two different features are observed for all spent catalysts with low I_S. The first feature at 934.2 ± 0.2 eV corresponds to Cu^{2+} as in the calcined catalysts, and the second feature at 932.6 ± 0.2 eV corresponds to Cu^+ and/or Cu^0 species. Cu^{2+} has a satellite feature due to its open-shell $3d^9$ configuration, while Cu^0/Cu^+ does not show a satellite due to its closed-shell configuration ($3d^{10}$). The intensity of main line also decreases from fresh to spent catalysts. A careful convolution (not shown) reveals that the intensity of the low-BE component increases with increase in x. $x = 0.5$@300 °C displays a high-intensity feature at 932.6 eV and a shoulder at 934 eV with a very weak satellite. This indicates that the

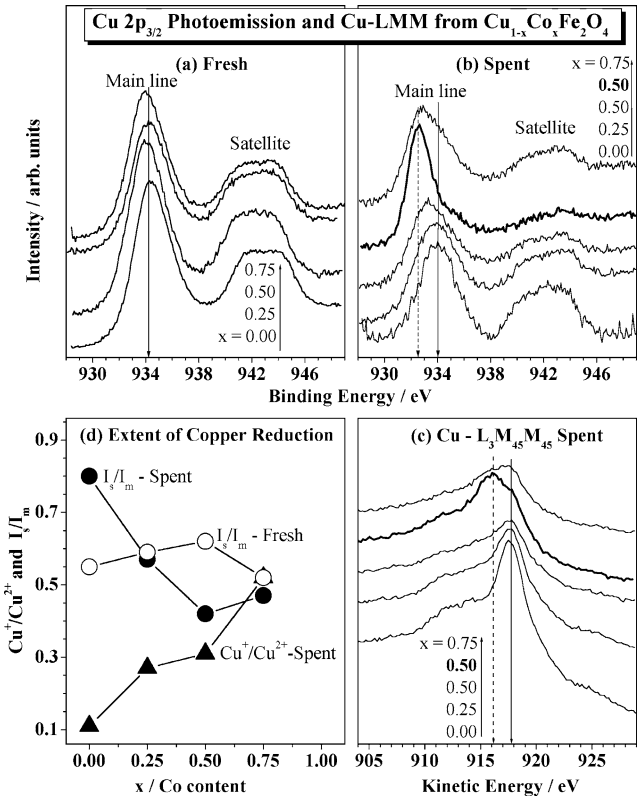

Fig. 4. Cu $2p_{3/2}$ photoemission spectra of (a) fresh and (b) spent $Cu_{1-x}Co_xFe_2O_4$ catalysts. Broadening on the lower-binding-energy side demonstrates a partial reduction of Cu^{2+} on spent catalysts. Cu $2p_{3/2}$ XPS of spent catalyst at a reaction temperature of 300 °C is also displayed in (b) to show the extent of the larger reduction due to higher temperature. (c) Cu $L_3M_{45}M_{45}$ Auger electron spectra from spent catalysts. (d) Satellite-to-main line intensity ratio (I_S/I_M) for fresh and spent catalysts and the ratio of Cu^+ to Cu^{2+} on spent catalyst. The reducibility of Cu increases with Co content.

high reaction temperature (300 °C) leads to a large reduction in Cu^{2+}.

Lower-valence Cu species can be distinguished by examining the Cu–$L_3M_{45}M_{45}$ Auger peaks shown in Fig. 4c. All the compositions exhibit a peak at a kinetic energy (KE) around 917.8 eV, characteristic of Cu^{2+} species. Additionally, a second component is also observed at about 916.2 eV and it is very intense on $x = 0.5$@300 °C, which is characteristic of Cu^+ species. It should be noted here that the KEs of the Cu–$L_3M_{45}M_{45}$ Auger peak values for Cu, CuO, and Cu_2O are 918.4, 917.6, and 916.5 eV, respectively [25,26]. Present KE values of 916.2 and 917.8 eV suggest contributions of Cu^+ and Cu^{2+} species, respectively, on spent catalysts and no Cu^0.

Fig. 4d shows the I_S/I_M ratios of fresh and spent catalysts and the reducibility of Cu. An important observation to be noted here is that the I_S/I_M ratio of spent catalysts decreases linearly from $x = 0.0$ to 0.5 and then increases marginally at $x = 0.75$; however, fresh catalysts display a value close to 0.55 and no significant change with x. It is also to be noted that the I_S/I_M ratio changes considerably from fresh to spent for $x = 0$ and 0.5 compositions; however, it remains

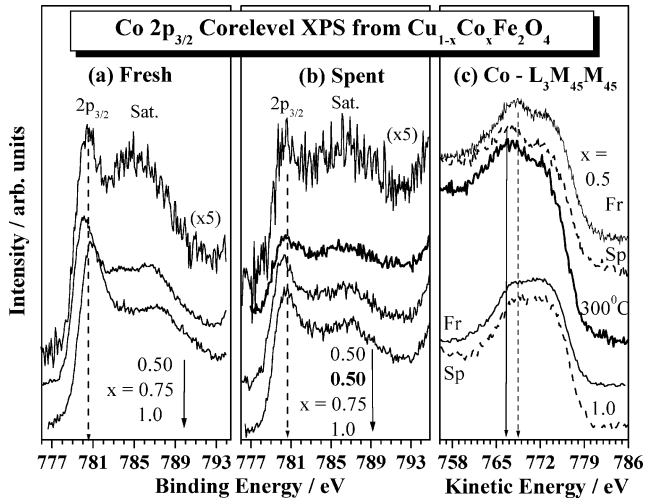

Fig. 5. Co $2p_{3/2}$ core-level photoemission spectra of (a) fresh and (b) spent $Cu_{1-x}Co_xFe_2O_4$ catalysts. (c) XAES from Co $L_3M_{45}M_{45}$ of fresh and spent $Cu_{1-x}Co_xFe_2O_4$ catalysts for $x = 0.5$ and 1. Co $2p_{3/2}$ XPS of spent catalyst at a reaction temperature of 300 °C is also displayed in (b) and (c) to show the effect of higher temperature in increasing surface Co concentration. The changes observed in intensity at $x = 0.5$ from fresh to spent catalysts are indicated by two arrows.

Table 3
XPS parameters from Co $2p$ core level in $Cu_{1-x}Co_xFe_2O_4$ catalysts

Composition, x	BE of Co $2p_{3/2}$ mainline (mainline–satellite energy gap, eV)	$2p_{3/2}$–$2p_{1/2}$ energy gap (eV)
$0.5^{F\,a}$	780.5 (4.7)	15.5
0.75^{F}	780.2 (3.4 and 6.1)	15.6
1.0^{F}	780.9 (4.6 and 6.1)	15.5
0.5^{S}	780.5 (6.2)	15.9
$0.5^{S\,(300\,°C)}$	780.2 (5.7)	16.0
0.75^{S}	780.4 (6.4)	15.8
1.0^{S}	780.5 (6.7)	15.9
CoO[b]	780.1±0.3	15.5
Co_2O_3[b]	779.6	–
Co_3O_4[b]	780.5	15.0

[a] Superscripts F and S indicate fresh and spent catalysts.
[b] Refs. [27–29].

the same for $x = 0.25$ and 0.75 compositions. Reducibility of Cu, calculated as the ratio of Cu^+ to Cu^{2+}, increases linearly with increasing Co content. This is totally contrary to a decrease in Cu reducibility for phenol methylation [21], and ethylation and isopropylation [22] reactions.

3.3.2. Co 2p core level and Co–L3M45M45

Co $2p_{3/2}$ photoemission spectra for fresh (a) and spent (b) catalysts are shown in Fig. 5 and the results are given in Table 3. The important features are: (1) the intensity of shakeup satellites decreases with increasing x; (2) the energy gap between the $2p_{3/2}$ peak and its satellite increases with increasing x on fresh and spent catalysts; and (3) an increase in the energy gap between Co $2p$ spin orbit doublets is observed from fresh to spent. Spent catalyst of $x = 0.5$@300 °C displays significantly high intensity features, indicating a higher Co concentration on the surface.

Table 4
Surface atomic ratio of fresh and spent $Cu_{1-x}Co_xFe_2O_4$ catalysts after *tert*-butylation reaction at 200 °C for 10 h

x	Fresh			Spent		
	Cu/Fe	Co/Fe	(Cu + Co)/Fe	Cu/Fe	Co/Fe	(Cu + Co)/Fe
0.00	1.17	–	1.17	0.68	–	0.68
0.25	1.04	0.20	1.24	0.74	0.16	0.90
0.50	0.79	0.32	1.11	0.68	0.40	1.07
				(0.44)[a]	(0.47)[a]	(0.91)[a]
0.75	0.50	0.50	1.00	0.44	0.45	0.89
1.00	–	0.75	0.75	–	0.66	0.66

[a] Results obtained from the sample subjected to phenol *tert*-butylation reaction at 300 °C for 10 h.

This is further corroborated by surface composition values (see above) (Table 4). High temperature leads to large segregation of Co^{2+} on the surface. Comparison of the BE values of catalysts with those of standard Co compounds (Table 3) clearly indicates the catalyst surfaces are in general composed of both Co^{2+} and Co^{3+}. A high I_S for $x = 0.5$ suggests contributions by Co^{2+} and high-spin Co^{3+}, since low-spin Co^{3+} shows poor I_s [27–29].

Co–$L_3M_{45}M_{45}$ Auger spectra of fresh and spent catalysts of $x = 0.5$ and 1 are shown in Fig. 5c exhibit broad features between 760 and 780 eV. Two features at around 767 and 772 eV are virtually the same for fresh and spent catalysts at $x = 1$. However, at $x = 0.5$, a shift in energy is observed for the lower-KE component on spent catalyst surfaces compared with fresh, and the shift is substantial for the catalyst exposed to 300 °C. Further, the high intensity indicates a large segregation of Co on the surface at 300 °C. $x = 0.75$ also shows characteristics similar to those $x = 0.5$.

3.3.3. *Fe 2p core level and Fe–$L_3M_{45}M_{45}$*

Fig. 6 shows the Fe $2p_{3/2}$ core level photoemission from (a) fresh and (b) spent $Cu_{1-x}Co_xFe_2O_4$ catalysts. There are two main differences between fresh and spent catalysts. (1) The main peak at 711 eV with a clear satellite at 718.5 eV due to Fe^{3+} is observed on fresh catalysts; I_S is relatively weak on spent catalysts and shifts to 719.5 eV. (2) Spent catalysts also indicate a shoulder around 709.6 eV, characteristic of Fe^{2+} species in tetrahedral coordination [30,31]; and the overall broadening observed for the satellites of all spent catalysts (except $x = 1$) supports contributions by both Fe^{3+} and Fe^{2+} [31]. Fig. 6c displays the Fe–$L_3M_{45}M_{45}$ spectra for $x = 0.5$ and 1.0 catalysts. Fresh catalysts are very similar and no difference is observed. There is a clear line broadening on the spent catalysts and a new low-KE feature appears as a shoulder on spent catalysts; however, it is not considerable at $x = 1$. A shoulder seen at 697.5 eV (broken line) on all spent catalysts is characteristic of Fe^{2+} species [21], and the lower intensity of this feature at $x = 1$ indicates the extent of Fe reduction might be low. $x = 0.5$@300 °C shows comparatively large intensity of Fe^{2+}, suggesting that high temperature induces large reduction. Fe $2p$ and Fe–LMM result indicate the partial reduction of Fe^{3+} to Fe^{2+} due to the phenol tertiary butylation reaction.

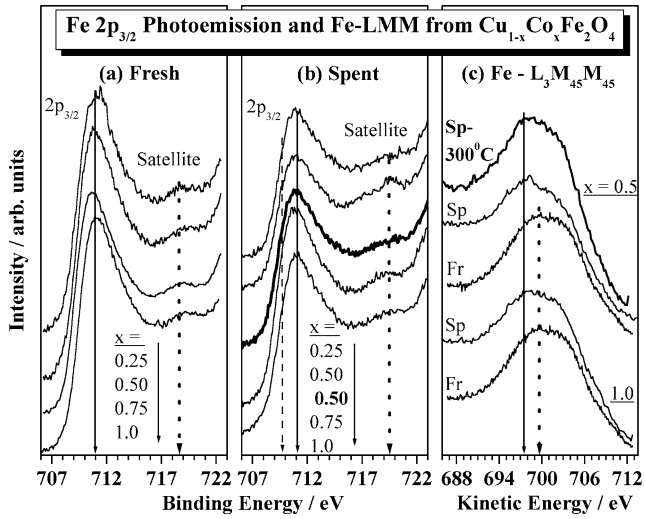

Fig. 6. Fe $2p$ core-level XPS of (a) fresh and (b) spent $Cu_{1-x}Co_xFe_2O_4$ catalysts. A clear shift is observed in satellite energy from fresh to spent catalysts (thick dotted arrows), and a weak shoulder seen below 710 eV on spent catalysts (broken line) for intermediate compositions ($0 < x < 1$) indicate partial reduction of iron. (c) XAES from Fe–$L_3M_{45}M_{45}$ of fresh and spent $Cu_{1-x}Co_xFe_2O_4$ catalysts for $x = 0.5$ and 1 compositions. Broadening due to an additional feature is denoted by a solid arrow and fresh catalyst feature is denoted by the thick dotted arrow.

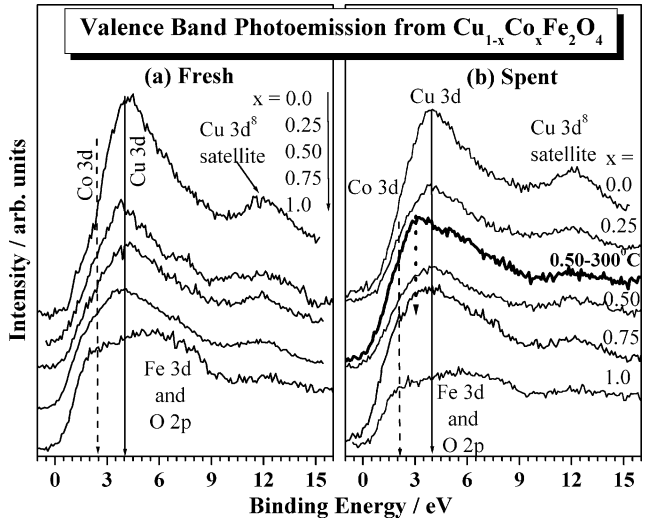

Fig. 7. Valence band XPS of (a) fresh and (b) spent $Cu_{1-x}Co_xFe_2O_4$ catalysts. The significant broadening of the valence band observed on spent catalysts is due to partial reduction of metal ions and consequent larger overlap of 3*d* energy bands of metal ions.

3.3.4. *Valence band photoemission*

Changes observed on spent catalysts from core level are reflected strongly in the valence band (VB) spectra too, shown in Fig. 7 with details. The main VBs observed have contributions predominantly from metal 3*d* bands below 10 eV and the assignments of various bands are from the photoionization cross-section values [32] at $h\nu = 1253.6$ eV and as explained earlier [21,22].

A few important observations are worth highlighting from the data: (1) The Cu 3*d* bands observed at 4.2 eV on

fresh catalysts (solid line) are found to be broadened on the lower-BE side toward the Co 3*d* region (broken line) on spent catalysts, indicating a reasonable overlap of energy bands of Cu and Co 3*d*. This is marked by a considerable dip in intensity between Cu and Co 3*d* bands on fresh catalysts and no such dip on spent catalysts. Additionally, on $x = 0.50$@300 °C, the 3*d* bands overlap is stronger in such a way that the Cu 3*d* band is shifted to 3 eV and the energy gap is just 1 eV between the Cu and Co 3*d* bands (dotted arrow, small). (2) The Cu $3d^8$ satellite appears on all the compositions containing Cu for fresh and spent catalysts; however, the satellite is more broadened with less intensity for intermediate compositions. (3) The shift in Fe 3*d* bands to lower BE is discernible on spent catalysts, except at $x = 1$. The shift in the trailing edge of VBs to lower BE to 7–8 eV, compared with 9 eV on fresh catalyst, testifies to the above. (4) There is a weak but finite photoemission intensity at E_F on spent catalyst (except $x = 1$), revealing the conducting nature of the catalyst. (5) Co 3*d* bands remain close to the same BE around 2.3 eV on fresh and spent catalysts. The preceding points illustrate an appreciable increase in the overlap of 3*d* energy bands on spent catalysts compared with fresh catalysts due to a partial reduction of metal ions.

3.3.5. Surface composition

Table 4 summarizes surface composition for both fresh and spent catalysts from XPS data. These data are extremely helpful in understanding the distribution and heterogeneity of metal ions on the surface, as it directly influences the catalytic activity. The important points to be noted from Table 4 are: (1) Generally, Cu/Fe and Co/Fe ratios change linearly with x on fresh as well as spent catalysts. (2) Cu + Co/Fe values indicates the spent catalysts are generally enriched with Fe compared with the respective fresh catalysts, except at $x = 0.5$, indicating the heterogeneity of the metal ions is maintained at a very high level on the surface. (3) Cu-rich compositions show a large decline in Cu/Fe on spent catalysts, whereas the Co/Fe ratio changes marginally from fresh to spent for all x values. (4) $x = 0.5$@300 °C and $x = 0.75$ show almost the same atomic ratio; this is further corroborated by the similar catalytic activity in Figs. 2b and 3a. This last point hints at the synergetic behavior between reaction temperature and catalyst composition. Coke depositions of 10–20%, depending on the reaction conditions and catalyst composition, were observed from the C 1*s* core level and thermogravimetric analysis (data not shown) [22].

Fig. 8 shows the interdependence of surface composition ((Cu + Co)/Fe) on the left panel and PhOH conversion with product yield on the right panel. It is clear from Fig. 8 that the heterogeneity dictates the catalytic activity to a large extent and the same is exemplified for the $x = 0.5$ composition which demonstrates a high phenol conversion and better product yield. This also hints at the importance of a 1:1 ratio of Cu to Co for the reaction. Albeit good heterogeneity for $x = 0.75$, the not so good activity is likely due to low

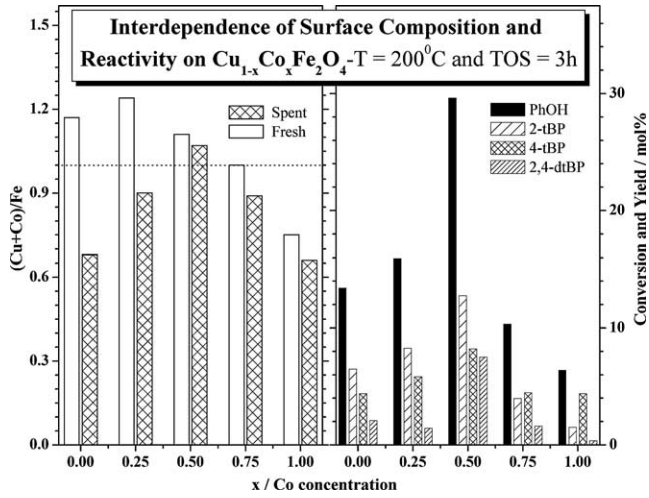

Fig. 8. Comparison of atomic ratio of Cu + Co/Fe for all compositions of fresh and spent catalysts (left panel) and phenol conversion and product yields on $Cu_{1-x}Co_xFe_2O_4$ catalysts at 200 °C, TOS = 3 h (right panel). Note the correlation between high heterogeneity and high catalytic activity for $x = 0.5$.

Cu and high Co content (Table 4). This is supported by the poor activity of Co-rich $x = 1$; however, $x = 1$ is selective to 4-tBP. Despite the Fe-rich surface for $x = 0$ and $x = 1$, the different reactivities are due to the Cu and Co species, respectively. Even through there are a few differences, $x = 0$ and $x = 0.25$ have comparable activity, indicating the importance of Cu to this reaction.

4. Discussion

4.1. Catalytic performance

From the activity data, it is evident that Cu-rich samples are active for tertiary butylation and Co-dominant compositions show poor activity, emphasizing the important role of Cu in this reaction. However, the equal bulk contents of Cu and Co at $x = 0.5$ show maximum activity and follow similar trends as in other phenol alkylations [21,22]. Except at $x = 0.5$, phenol conversion is between 5 and 16 mol% for all other compositions, suggested that tertiary butylation activity is due mainly to the Cu + Co combination, of which Cu is highly active. An important aspect of the butylation reaction is related to product selectivity too. At an optimum temperature of 200 °C, IB attaches to the phenolic ring to give *tert*-butyl phenols. Unlike lower alkylations, tertiary butylation of phenol gives three major products, namely, 2-tBP, 4-tBP, and 2,4-dtBP, and the selectivity of each product depends on the various reaction parameters. The total *ortho* selectivity observed with any composition is $\leqslant 50\%$, whereas phenol methylation and ethylation are noted for high *ortho* selectivity of $> 90\%$ [21,22]. Two reasons are the bigger size and higher stability of t-butyl species compared with other lower alkyl species, and hence it is worth analysis by in situ spectroscopy methods. Further, the linear change observed

between phenol conversion and 2,4-dtBP selectivity under most conditions hints that 2,4-dtBP production is controlled by first-order dependent phenol conversion and sequential butylation of 2-tBP. High 4-tBP selectivity on $x = 0.5$ at high IB:PhOH ratio (Fig. 2a) indicates the surface could be dominated by Co, as in $x = 0.5$@300 °C.

From WHSV studies it is clear that the selectivities of 2-tBP and 2,4-dtBP show reverse trends with a changing contact time. Due to long contact time sequential alkylation is increasingly feasible at low WHSV and entirely supports the high selectivity of 2,4-dtBP at low WHSV. The foregoing facts indicate the reaction is kinetically controlled and product distribution can be optimized. Further, they also demonstrate an increase in the selectivity of 2,4-dtBP at the expense of 2-tBP. An increase in 2-tBP selectivity with increasing WHSV indicates that 2-tBP is preferred over other products at short contact time, probably due to phenol orientation on the catalyst surface, which is easily *ortho*-butylated. Possible dealkylation reactions at higher temperatures may also account for a decrease in the selectivity of 2,4-dtBP. Lower t-butylation activity at higher temperatures is due to the side reactions of IB with to butylenes and aliphatics.

4.2. Reaction mechanism

A detailed investigation of the acid–base properties of the $Cu_{1-x}Co_xFe_2O_4$ catalyst system was carried out separately [23]. Important points from FT-IR studies help in gaining an understanding of tertiary butylation activity: (1) The $Cu_{1-x}Co_xFe_2O_4$ surface is dominated by Lewis acid character. (2) A relatively weak acidic character at $x = 0$ increases with Co content to highly acidic character at $x = 1.0$ with an increase in number and strength of acidic sites (Table 1). (3) The basic character of the catalyst decreases with increasing x. (4) The acid–base character on the catalyst surface is due predominantly to octahedral cations, and the Lewis acidity changes significantly depending on the easily reducible (Cu^{2+}) or nonreducible (Co^{2+}) ions in the neighborhood. Generally, robust Co^{2+} in the neighborhood increases the acidity. A simple comparison of phenol conversion and acid–base character demonstrates that neither strong acidic nor strong basic character helps the tertiary butylation reaction. It is also evident that the intermediate acid–base character observed for the $x = 0.5$ composition (Tables 1 and 2) with high catalytic activity indicates an optimum level of acid–base sites are required for better catalytic performance in terms of phenol conversion and overall product yield. Strong acidity promotes oligomerization and cracking of IB; thus the conversion of phenol is expected to be lower, which is the case with Co-rich compositions (Fig. 2b). In addition, butyl phenols may also undergo dealkylation in the presence of strong acid sites, accounting for the low conversion of phenol at $x \geqslant 0.75$. However, the highly acidic property at $x = 1$ improves 4-tBP selectivity. It is in agreement that strong acid sites favor 4-tBP and weak to moderate acid sites favor 2-tBP as in zeolites [11] and mesoporous materials [7,9]. However the requirement for strong acidic sites for 2,4-dtBP on the above-mentioned material is contrary to the present results, suggesting the p-*tert*-butylation mechanism is different on ferrites. It is to be noted that the catalyst having intermediate acid–base character ($x = 0.5$) has maximum yields of 2,4-dtBP and 2-tBP.

Alkylation of phenols, just like other aromatic compounds, follows the Friedel–Kraft mechanism. From electrophilic substitution it is clear that the *tert*-butyl cation attacks the phenol ring preferentially in positions *ortho* and/or *para* to the –OH group. The ratio of isomers formed initially is kinetically controlled and is determined by phenolic OH groups and incoming *tert*-butyl cations in the present case. Though the mono-*tert*-butylated phenols are more active than phenol, subsequent tertiary butylation occurs only when there is less steric hindrance.

Phenol is adsorbed as phenolate by dissociative adsorption on an acid–base site. Simultaneously, protonation of IB occurs due to H^+ from the above process. The protonated IB rearranges to give an appreciably stable *tert*-butyl cation, which in turn attacks phenoxide either from the adsorbed or gaseous state. The relatively high selectivity of 2-tBP than 4-tBP indicates that the carbocation attacks preferentially from the adsorbed state. However, high Co content reverses the above trend and favors *para*-*tert*-butylation probably from gas phase. FT-IR investigation of phenol methylation with methanol on $Cu_{1-x}Co_xFe_2O_4$ shows exclusive *ortho*-alkylation, due to the close proximity of the *ortho* positions of phenoxide to the catalyst surface, compared with the para positions [33]. Once formed, 2-tBP acts as a precursor to the formation of 2,4-dtBP. Nonetheless, steric hindrance of the *tert*-butyl group prevents the further attack by IB at the *ortho* position of already formed 2-tBP, illustrating negligible formation of 2,6-dtBP. In addition, once the 2-tBP forms, the phenyl ring cannot be coplanar to the catalyst surface due to the bulky size of the t-butyl group, indicating the *para* position of the phenyl ring is far removed from the surface and supported by negligible second *ortho* tertiary butylation. However, the *tert*-butyl cation can attack, from the gaseous state, phenol or 2-tBP, resulting in the formation of 4-tBP and 2,4-dtBP, respectively. This is in contrast to the reaction between phenol and any alcohol where the formation of *para* alkylated product is $< 1\%$ [22]. Tertiary butylation of phenol has been carried out with *tert*-butyl alcohol and the conversion was found to be $\leqslant 5\%$ under any condition and hardly any 4-tBP was detected [22]. This clearly indicates that both IB and *tert*-butyl alcohol in the adsorbed state might not produce any p-alkylated product over the present catalyst system. The above results and discussion hint that both Hinshelwood and Eley–Rideal mechanisms are possible for tertiary butylation on $Cu_{1-x}Co_xFe_2O_4$.

4.3. Electronic structure aspects

That (phenol + IB) creates a reducing atmosphere is confirmed by the observation of H_2, CO, and cracked products

of IB in gaseous products. The XRD pattern of spent catalysts obtained at 200 °C shows Cu^0 on $x = 0$; however, only a trace amount is detected on other catalyst compositions. An optimum temperature of 200 °C is not capable of accelerating the reduction process is very much reflected in the XRD and XPS results. Fe carbides, Fe^0, and Cu^0 detected in the methylation and ethylation spent catalysts [21,22] are not detected in the XRD pattern of tertiary butylation spent catalysts. Nevertheless, the unreacted phases of CuO and α-Fe_2O_3 present on the fresh catalyst at $x = 0$, which remain after the reaction to some extent, could be the reason for sizable amounts of Cu^0 and Fe_2O_3. This contrasts with the observation of magnetite on spent catalysts ($x = 0$) after methylation and ethylation [21,22] between 300 and 400 °C.

The changes observed on main peaks, satellites, and Auger features of Fe, Co, and Cu are a clear-cut indication that partial reduction of these species occurs during the reaction. It is useful to highlight the following observations from XPS: (1) Copper reduction is seen for $x \leqslant 0.75$ and the extent of reduction increases linearly with X as well as reaction temperature. (2) There is partial reduction of all metal ions and a consequent increase in the overlap of 3*d* energy bands in the spent catalysts, especially at intermediate compositions. (3) The (Cu + Co)/Fe ratio at $x = 0.5$ remains around 1.1 before and after reaction. Thus, a high phenol conversion and a Cu + Co/Fe ratio close to 1 at $x = 0.5$ ensure the optimum distribution of active species to have a highly heterogeneous surface. The high activity observed at $x = 0.5$ highlights the importance of a 1:1 bulk ratio of Cu:Co. The above also suggests that the surface atomic ratio remains almost the same throughout the reaction period on $x = 0.5$, but the low activity at a TOS of 10 h is due mainly to coke deposition. Apparently the coke deposition merely decreases the percentage of metal ion on the surface, but not the metal ion ratio significantly and hence the above observation. This also suggests that coke formation does not affect other results significantly for $x = 0.5$. Simple calcination in air restores the original activity. A change from low activity observed at $x = 1$ to better activity at $x \leqslant 0.75$ indicates the importance of Cu^{2+} for better performance.

The extent of Cu reducibility increases with increasing x on spent catalysts. This is in excellent agreement with the results obtained from temperature programmed reduction (TPR) of $Cu_{1-x}Co_xFe_2O_4$ in H_2 atmosphere [20]. Two important reduction processes involved are $Cu^{2+} \rightarrow Cu^+$ and $Cu^+ \rightarrow Cu^0$, at increasing temperature between 180 and 280 °C. $Cu^{2+} \rightarrow Cu^+$ occurs around 200 °C and the amount of H_2 consumed increases with x. Additionally, a gradual decrease in the reduction temperature is observed for $Cu^+ \rightarrow Cu^0$ as x increases. Since the tertiary butylation of phenol is carried out at 200 °C, which is at the $Cu^{2+} \rightarrow Cu^+$ reduction temperature, the decrease in $Cu^+ \rightarrow Cu^0$ reduction temperature also favors the above. The preceding TPR results entirely support increasing Cu reducibility with increasing x at 200 °C as observed in XPS.

XPS studies on spent catalysts of $Cu_{1-x}Co_xFe_2O_4$ revealed that Cu and Co 3*d* energy bands overlap to a considerable extent and play an important role in catalytic performance. The relatively strong overlap of 3*d* energy bands of metal ions in methylation and ethylation reactions compared with tertiary butylation is due mainly to the high temperature (350–375 °C) employed in the former cases compared with 200 °C in the latter.

5. Conclusions

This article reports the results from the catalytic study of tertiary butylation of phenol with isobutene on $Cu_{1-x}Co_xFe_2O_4$ as a function of various reaction parameters and catalyst compositions. Fresh and spent catalysts were subjected to detailed analysis by XRD, XPS, and XAES. Phenol tertiary butylation gives three major products, namely, 2-tBP, 4-tBP, and 2,4-dtBP, and the phenol conversion and selectivity of these products depend on the reaction conditions. It is found that $x \leqslant 0.5$ compositions are comparatively more active, indicating the importance of Cu for this reaction. $x = 0.5$ shows better activity, emphasizing the importance of the 1:1 bulk combination of Cu + Co for overall performance.

It is found that the acid–base properties of the system have considerable influence on product selectivity. A large number of strong acid sites on $x = 1$ does help in the formation of 4-tBP. On the other hand, the selectivities of 2-tBP and 2,4-dtBP are lowest on catalysts with strong acidity; however, catalysts having intermediate acid–base property have maximum products yield. The high activity achieved with $x = 0.5$ demonstrates that an optimum concentration of acid–base centers is needed for phenol adsorption and subsequent polarization of both phenol and the alkylating agent. In phenol alkylation with isobutene, the tertiary butyl carbocation can attack, from the adsorbed as well as the gaseous state, the phenol, resulting in the formation of *para* tertiary butylated products such as 4-tBP and 2,4-dtBP. Steric hindrance of the *tert*-butyl group prevents the further attack of IB at the *ortho* position of already formed 2-tBP, illustrating negligible formation of 2,6-dtBP.

XPS analysis of both fresh and spent $Cu_{1-x}Co_xFe_2O_4$ catalysts indicates that the oxidation states of the metal ions and their distribution on the surface have considerable influence on activity and selectivity toward phenol tertiary butylation. XRD and XPS studies reveal that redistribution as well as partial reduction of metal ions occurs to various levels due to reaction. The high activity at $x = 0.5$ demonstrates that uniform distribution of reactive Cu species with heterogeneous neighbors of Co and Fe is essential. Valence band studies show a change from marginal overlap between 3*d* bands of metal ions on fresh catalysts to a significant overlap on spent catalysts. It is clear that the $x = 0.5$ catalyst brings out synergetic behavior due to 3*d* energy band overlap and an intermediate acid–base character and enhances catalytic

activity. It is likely that a combination of all the factors—optimum acid–base character, relatively high surface area, uniform distribution of active species with heterogeneous neighbors, and 3*d* bands overlap—contributes to overall reactivity and further quantitative experiments are necessary to single out the factor that contributes the most to activity.

Acknowledgment

T.M. thanks CSIR, New Delhi, for a senior research fellowship.

References

[1] H.-W. Voges, in: B. Elvers, S. Hawkins, G. Schulz (Eds.), Ullmann's Encyclopedia of Industrial Chemistry, vol. A19, VHC, Weinheim, Germany, 1991, p. 328.
[2] M. Inoue, S. Emoto, Chem. Pharm. Bull. 20 (1972) 232.
[3] S. Velu, C.S. Swamy, Res. Chem. Intermed. 26 (2000) 295.
[4] A. Sakthivel, N. Saritha, P. Selvam, Catal. Lett. 72 (2001) 225, references therein.
[5] K.G. Chandra, M.M. Sharma, Catal. Lett. 19 (1993) 309.
[6] R.A. Rajadhyakasha, D.D. Chaudhari, Ind. Eng. Chem. Res. 26 (1987) 1276.
[7] S.K. Badamali, S. Sakthivel, P. Selvam, Catal. Lett. 65 (2000) 153.
[8] K. Zhang, H. Zhang, G. Xu, S. Xiang, D. Xu, S. Liu, H. Li, Appl. Catal. A 207 (2001) 183.
[9] S.K. Badamali, S. Sakthivel, P. Selvam, Catal. Today 63 (2000) 291.
[10] S. Subramanian, A. Mitra, C.V.V. Satyanarayana, D.K. Chakrabarty, Appl. Catal. A 159 (1997) 229.
[11] K. Zhang, C. Huang, S. Xiang, S. Liu, D. Xu, H. Li, Appl. Catal. A 166 (1998) 89.
[12] A.H. Padmasri, V.D. Kumari, P.K. Rao, Stud. Surf. Sci. Catal. 113 (1998) 563.
[13] J.W. Yoo, C.W. Lee, B. Wang, S.E. Park, Res. Chem. Intermed. 27 (2001) 561.
[14] M. Nagai, T. Yoda, M. Kodomari, J. Catal. 201 (2001) 105.
[15] R. Rajgopal, R. Vetrivel, B.S. Rao, Catal. Lett. 65 (2000) 99.
[16] K. Sreekumar, T. Mathew, S.P. Mirajkar, S. Sugunan, B.S. Rao, Appl. Catal. A 201 (2000) L1.
[17] K. Sreekumar, T. Mathew, B.M. Devassy, R. Rajagopal, R. Vetrivel, B.S. Rao, Appl. Catal. A 205 (2001) 11.
[18] K. Sreekumar, T.M. Jyothi, T. Mathew, M.B. Talawar, S. Sugunan, B.S. Rao, J. Mol. Catal. A 159 (2000) 327.
[19] B.S. Rao, K. Sreekumar, T.M. Jyothi, Indian Patent 2707/98 (1998).
[20] K. Lázár, T. Mathew, Z. Koppány, J. Megyeri, V. Samuel, S.P. Mirajkar, B.S. Rao, L. Guczi, Phys. Chem. Chem. Phys. 4 (2002) 3530.
[21] T. Mathew, N.R. Shiju, K. Sreekumar, B.S. Rao, C.S. Gopinath, J. Catal. 210 (2002) 405.
[22] T. Mathew, Synthesis and Characterization of Mixed Oxides Containing Cobalt, Copper and Iron and Study of Their Catalytic Activity, PhD thesis, University of Pune, 2002.
[23] T. Mathew, N.R. Shiju, B.B. Tope, S.G. Hegde, B.S. Rao, C.S. Gopinath, Phys. Chem. Chem. Phys. 4 (2002) 4260.
[24] G. Moretti, G. Fierro, M.L. Jacono, P. Porta, Surf. Interface Anal. 14 (1989) 325.
[25] S. Poulston, P.M. Parlett, P. Stone, M. Bowker, Surf. Interface Anal. 24 (1996) 811.
[26] B.R. Strohmeier, B.E. Leyden, R.S. Field, D.M. Hercules, J. Catal. 94 (1985) 514.
[27] M.S. Stranick, M. Houalla, D.M. Hercules, J. Catal. 106 (1987) 362.
[28] N.S. McIntyre, M.G. Cook, Anal. Chem. 47 (1975) 2210.
[29] Z. Zsoldos, L. Guczi, J. Phys. Chem. 96 (1992) 9393.
[30] P. Mills, J.L. Sullivan, J. Phys. D 16 (1983) 723.
[31] T. Fujii, F.M.F. de Groot, G.A. Sawatzky, F.C. Voogt, T. Hibma, K. Okada, Phys. Rev. B 59 (1999) 3195.
[32] J.J. Yeh, I. Lindau, Atom. Data Nucl. Data Tables 32 (1985) 1.
[33] T. Mathew, S. Pai, B.B. Tope, S.G. Hegde, B.S. Rao, C.S. Gopinath, J. Phys. Chem. B, submitted.